# Experimental evidence for a virtual state in a cold collision: Electrons and carbon dioxide

D. Field,[1,*] N. C. Jones,[1] S. L. Lunt,[1] and J.-P. Ziesel[2]
[1]*Institute of Physics and Astronomy, University of Aarhus, DK-8000 Aarhus C, Denmark*
[2]*Laboratoire Collisions Agrégats Réactivité (CNRS UMR5589), Université Paul Sabatier, 31062 Toulouse, France*
(Received 21 November 2000; published 9 July 2001)

Experimental data are presented for the scattering of cold electrons by $CO_2$, for both integral and backward scattering, down to energies of a few meV with an energy resolution of 0.95–1.5 meV (full width at half maximum) in the electron beam. The experimental data show evidence for the phenomenon of virtual-state scattering, a subject of extensive theoretical study. The measured scattering cross sections rise rapidly at low energy, to a limiting value in integral scattering in excess of 120 Å$^2$. In addition, analysis shows that scattering is *s*-wave dominated and that the *s*-wave scattering length is negative. All features are characteristic of virtual state scattering.

DOI: 10.1103/PhysRevA.64.022708 PACS number(s): 34.80.−i

## I. INTRODUCTION

Cold collisions, in which the de Broglie wavelength is very much greater than the typical size of a molecule [1], form a fascinating topic, since quantum effects dominate the outcome of the collisions. Here we report the results of cold electron-scattering experiments, which provide experimental evidence for the existence of a so-called ''virtual state'' [2,3,4]. The first rigorous theoretical demonstration of virtual-state scattering was reported recently in Ref. [2]. The presence of a virtual state causes $CO_2$ to be extraordinarily efficient in scattering low-energy electrons. Our data point the way to a set of cold collisional phenomena due to virtual states, relating both to electron-molecule interactions involving large polarizable species and also heavy particle collisions relevant to the formation of Bose-Einstein molecular condensates [1,5].

The study of cold collisions involving molecules is a subject in its infancy and new phenomena remain to be identified and characterized experimentally. The virtual-state phenomenon is a prime example. Virtual states arise in theoretical models as states of the collision partners in the continuum and are dubbed virtual because they cannot be accessed classically on grounds of energy conservation. Theory suggests that virtual states may have a dramatic effect on scattering, enhancing elastic cross sections by factors that may approach two orders of magnitude in low-energy encounters. Below we describe experiments that demonstrate the reality of the virtual-state phenomenon. The experimental system, which we use for these studies, is uniquely able to control low-energy electron beams and perform scattering experiments down to kinetic energies below 10 meV. Electrons at these energies are represented by matter waves of long wavelength, for example, of 12.2 nm at 10 meV energy or 120 K. For comparison, a Rb atom at a temperature of $5\times10^{-4}$ K has the same wavelength. Thus understanding of quantum events in electron scattering at very low energies contributes to an understanding of cold atom and molecule scattering, a theme to which we return briefly at the end of this paper.

The choice of $CO_2$ as a target species in the present work arose partly because of its intrinsic interest and partly because theory, based originally upon model potentials [6], and supported by some early experiments [7], has long suggested that electron-scattering cross sections are anomalously high at low collision energies. Electron collisions with $CO_2$ have become the virtual-state test bed and new supercomputing resources have signaled a major recent and on-going computational effort to investigate the system. These *ab initio* studies [2,3,4,8,9,10] have given strong support to the view that a virtual state is created at low energy, in which a bound state of the electron and $CO_2$ is almost, but not quite, born. Our investigations with cold electrons extend down to energies an order of magnitude lower than any previous measurements and also provide directly the backward-forward asymmetry of the scattering. The latter information is essential in order to establish the nature of electron-$CO_2$ scattering and the present data furnish telling experimental evidence for the existence of this delicate quantum creature, the virtual state.

## II. EXPERIMENTAL METHOD

In our experiments, see for example [11], synchrotron radiation from the ASTRID storage ring at the University of Aarhus provides an electron source through photoionization of argon. The wavelength of the synchrotron radiation is tuned to the sharp autoionizing resonance Ar** $3p^5(^2P_{1/2})11s$ superposed on the broad $9d'$ resonance at 78.65 nm [12], a few meV above the ionization energy threshold for $^2P_{3/2}$ $Ar^+$ at 15.759 eV (78.676 nm [12]). The resulting photoelectrons have an energy resolution which is determined by the energy resolution in the photon beam. The undulator beamline on ASTRID, fitted with a spherical grating monochromator, delivers photons, and therefore photoelectrons, with a resolution as high as 0.75 meV full width at half maximum (FWHM). Doppler motions of the room-temperature target gas degrade the effective energy resolution in the present experiments by less than 1% for collisions at 10 meV impact energy, rising to ~15% at 100 meV [13].

*Corresponding author. Email address: dfield@ifa.au.dk

 

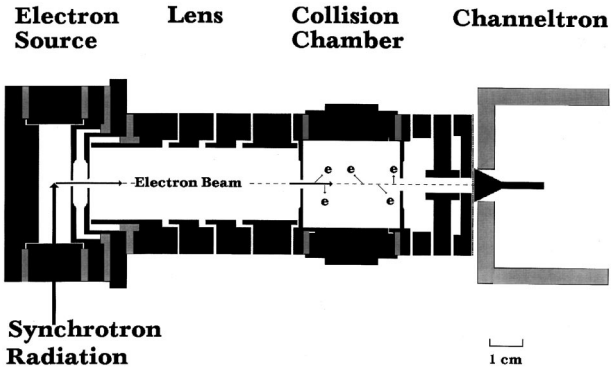


FIG. 1. A scale diagram of the apparatus. Monochromatic synchrotron radiation enters a photoionisation source containing argon. Photoelectrons, expelled by a weak electric field, are focused by a four-element lens [14] into a collision chamber containing $CO_2$. Transmitted electrons are detected at the channel electron multiplier (''channeltron'') situated beyond some further electron optics.

Figure 1 shows a scale diagram of the apparatus. Synchrotron radiation is focused at the center of the region of photoionization into the form of a strip less than 10 $\mu$m in thickness, representing a demagnified image of the exit slit of the monochromator. A weak electric field expels the electrons from the source region. Electrons are formed into a beam and focused by a four-element electrostatic zoom lens [14] into a cell containing the target gas at room temperature. The energy of the beam is scanned by varying the potential in the electron source region. The attenuation of the beam in the presence of the target gas is measured as a function of electron energy by recording the beam intensity at a channel electron multiplier (Galileo channeltron 7010M) beyond some further electron optics. The entire system may be immersed in an axial magnetic field [11] of strength $\sim 2 \times 10^{-3}$ T.

The cross-section for scattering is given by $(Nl)^{-1} \ln(I_0/I_t)$, where $N$ is the target gas number density, $l$ is the path length in the gas, and $I_0$ and $I_t$ are, respectively, the intensities of the incident and transmitted electron beams. Measurement of pressure was performed using a Leybold Viscovac VM212 rotating-ball gauge. Extensive comparison with data from other laboratories has shown that the path length $l$ is the geometrical length (=30 mm) of the scattering cell. When the magnetic field is absent, the measured cross section is the total integral scattering cross section, where ''total'' refers to all elastic and inelastic events and ''integral'' refers to integration over the full $4\pi$ sr. In separate measurements, with the magnetic field present, only backward-scattered electrons are recorded as lost to the incident beam, since forward-scattered electrons are guided onto the detector. The cross section measured is the total backward-scattering cross section, that is, the cross section for all events that cause electrons to be scattered into the backward $2\pi$ sr. The performance of the instrument in measuring backward-scattering cross sections has been extensively checked [11,15] by comparison with known data. Calibration of the absolute electron kinetic energy, necessary due to contact potentials of typically tens of millivolts, is performed using energy-calibrated scattering spectra for $N_2$ [16] and $O_2$ [15] (and references therein). The electron energy can be specified with an uncertainty at higher energies of $\pm 5$ meV. Zero energy may also be clearly identified from the onset of detectable current and at the very lowest energies the absolute scale is known with an uncertainty of better than $\pm 1.5$ meV. The uncertainty in reported cross sections due to random errors in the measurements is estimated to be $\pm 8\%$ (one standard deviation) at the lowest energies, falling to $\pm 5\%$ at higher energies, that is, above 100 meV. These estimates take into account uncertainties in pressure measurements, random fluctuations in the measured electron-beam intensities and uncertainties in our calibrations and in data from other laboratories with which comparison was made (see above).

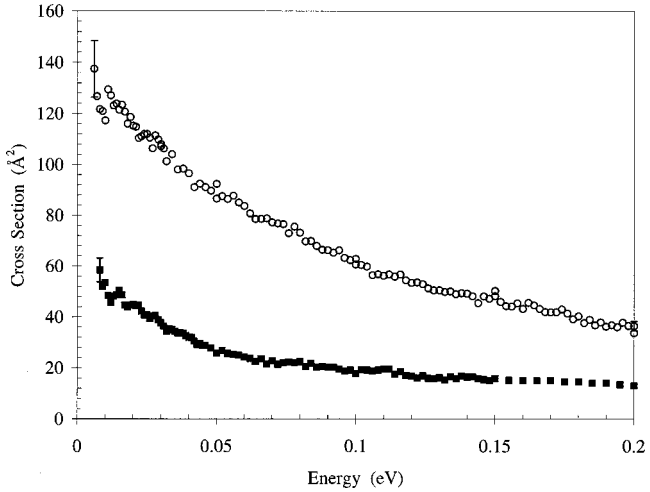


FIG. 2. Experimental scattering cross sections for electrons and $CO_2$ vs electron impact energy. The upper set of data are total integral scattering cross sections, and the lower, total backward cross sections. Errors in the values of cross sections are $\pm 5\%$ between 30 and 200 meV increasing to $\pm 8\%$ for lower energies. The slight tendency to oscillation in the backward cross sections is an experimental artifact.

## III. RESULTS AND DISCUSSION

Our experimental results are shown in Fig. 2. The energy resolution (FWHM) in the incident electron beam was set to 0.95 meV above 50 meV impact energy and 1.5 meV below this energy. For $CO_2$, the processes that may contribute to the measured cross sections are elastic scattering, quadrupole-induced rotationally inelastic scattering, and vibrationally inelastic scattering. Analysis of rotationally inelastic collisions [17,18] shows that these have integral cross sections of 1.2–1.4 Å$^2$. Vibrationally inelastic collisions [19,20] with thresholds at 82, 172, and 292 meV for the bend, symmetric, and asymmetric stretch, respectively, have integral cross sections at maximum of the order of 1–1.5 Å$^2$. Hence inelastic contributions to the measured cross sections in Fig. 2 can be ignored to within the experimental error of measurement (see caption to Fig. 2) at impact energies below, say, 100 meV. Figure 3 shows a comparison between theoretical values, for elastic scattering, and experimental data, including the two other measurements available of ab-

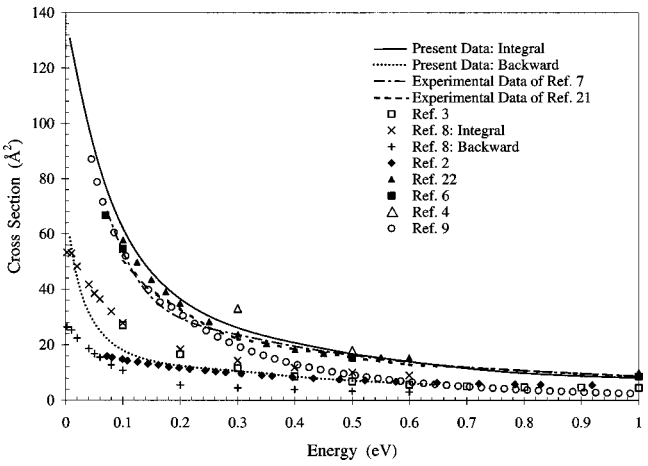


FIG. 3. Comparison between experiment and theory: for clarity experimental values are shown as continuous, dashed, and dotted lines and theoretical estimates as symbols. All theoretical values save [6] and [22] are *ab initio.*

solute cross sections below a few hundred meV [7,21]. All theories are *ab initio* studies save for two early model potential calculations [6,22]. Very recent work [3,4,8,9,10] provides qualitative confirmation of the findings in the first *ab initio* study [2]. All theories show the characteristic increase in cross section at low energy and all attribute this to virtual-state scattering. Theoretical results in [8] demonstrate backward-forward symmetry in the angular variation of the scattering at low energy, pointing to the dominance of *s*-wave scattering. The inaccuracy of *ab initio* theoretical values, and the discrepancies between them, arise from the well-known and very considerable difficulties involved in treating correlation and exchange in low-energy electron collisions.

A physical description of virtual-state scattering is as follows. The electron-$CO_2$ interaction yields an energy well, which may support states of $CO_2^-$. Depending on the strength of the interaction, such states may, in principle, be bound or lie in the continuum, a little above the top of the well. The latter give rise to virtual-state scattering. If such a state in the continuum differs by an energy $\Delta E$ from the total energy of the system, then the electron wave in the presence of $CO_2$ feels the influence of the state for the brief period $\Delta t$ where $\Delta E \Delta t \geqslant h/2\pi$. Calculations [23] suggest that $\Delta t$ is of the order of $10^{-15}$ s. The presence of this state gives additional phase shift to the scattered electron wave. The smaller the energy mismatch $\Delta E$, the greater is the cross section in the limit of low energy. Virtual-state scattering does not lengthen the lifetime of the electron-molecule encounter and is therefore not resonant scattering. Moreover only *s* waves give rise to the virtual state effect, which peaks as the impact energy approaches zero. If higher angular momentum waves are involved, shape resonances, for example, may be formed above zero energy, involving states of $CO_2^-$ in the continuum. We show below that higher angular momentum waves are not significantly involved here. In addition, the electronic symmetry of the $CO_2^-$ state in the continuum may exclude the *p* wave from involvement in scattering. Feshbach resonances involving *s* waves, or higher *l* waves if states of suitable symmetry are available, could also, in principle, be encountered.

Our data show that the electron-$CO_2$ scattering cross section rises to an anomalously high limiting value at very low energy, as expected for virtual-state scattering. The angular information in our data in Fig. 2 is used below to demonstrate that the rise in cross section at low energy does not have a strong contribution from, say, a *p*-wave resonance but rather is strongly *s*-wave dominated. We have noted that this is an essential characteristic of virtual-state scattering. The angular variation of scattering at our lowest experimental energy is approximately 60% forward and 40% backward. Pure *s*-wave scattering would yield symmetrical backward-forward scattering. Our data therefore indicate some residual *p*-wave component, that is, $l=1$ waves contributing to backward-forward asymmetry. We now show that the *p*-wave component is in fact very small and that at energies around 10 meV, scattering is indeed very close to pure *s* wave. Two approximations are introduced, in the first place that only *s*- and *p*-partial waves contribute to the scattering, a good approximation at low energies, and in the second that the interaction potential of electrons with $CO_2$ is spherically symmetrical. With respect to the latter approximation, the spherically symmetrical charge-induced dipole potential remains more than twice as powerful as the angle-averaged charge-permanent quadrupole moment potential out to a range of interaction of 5 Å. Without any assumptions about the mechanism of scattering or the radial dependence of the electron-$CO_2$ interaction potential, it follows on the basis of these approximations that the integral and backward-scattering cross sections, $\sigma_T$ and $\sigma_B$, respectively, may be represented in terms of the shifts of phase that the *s* and *p* waves undergo in the course of scattering from the target, as follows [15]

$$\sigma_T = \frac{4\pi}{k^2}(s^2+3p^2) \tag{1}$$

$$\sigma_B = \frac{2\pi}{k^2}[(s^2+3p^2)-3\{s^2p^2+sp[(1-s^2)(1-p^2)]^{1/2}\}], \tag{2}$$

where $s \equiv \sin\eta_0$ and $p \equiv \sin\eta_1$, $\eta_0$ and $\eta_1$ are, respectively, the *s*- and *p*-wave phase shifts. **k** is the wave vector whose magnitude is given by $k=(2E)^{1/2}$, where $E$ is the electron impact energy in a.u. In order to extract phase shifts we have expressed these as expansions in $k$. Expansions up to $k^4$ are more than adequate to extract values of $\eta_0$ and $\eta_1$ within the accuracy of the experimental data. The coefficients of powers of $k$ in expansions for *s*- and *p*-wave phase shifts have been varied so as to reproduce as closely as possible our experimental data on a least-squares basis, using Eqs. (1) and (2). This simple fitting procedure, ''partial-wave fitting,'' yields a set of absolute values *s*- and *p*-wave phase shifts, modulo $\pi$, as a function of impact energy. In order to limit the inaccuracy associated with inclusion of only *s* and *p* waves, data were fitted to energies only up to 100 meV. We find that the *s*-wave contribution to the scattering is strongly dominant at our lowest experimental energies. As an ex-

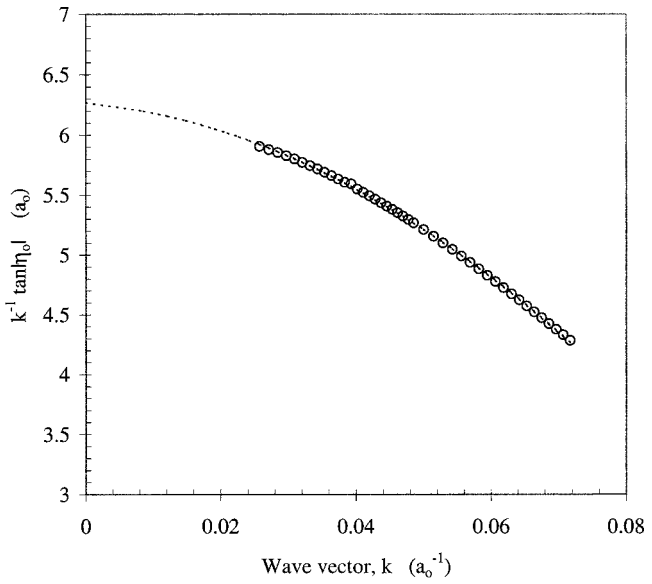


FIG. 4. The variation of $\mathbf{k}^{-1}\tan|\eta_0|$, shown as open circles, vs **k**, where **k** is the wave vector, expressed in atomic units (per Bohr radius $a_0$), and $\eta_0$ is the *s*-wave phase shift estimated from a fit to the experimental data of Fig. 2. The dotted line represents the fit by which the value of the intercept on the ordinate was determined. The intercept gives the absolute value of the scattering length in units of $a_0$.

ample, the *s*-wave phase shift is $|0.158|\pm0.002$ rad at 10 meV, contributing 118.5 Å$^2$ to the integral scattering cross section. The *p*-wave phase shift is approximately an order of magnitude lower, contributing the additional few Å$^2$ to make up the total recorded in Fig. 2. The data are of insufficient quality to provide better than an order of magnitude estimate of the *p*-wave phase shift, but the dominance of *s*-wave scattering is quite evident. Our derived phase shifts also show that the proportion of the cross section attributable to *p* waves relative to *s* waves drops at lower energy, as the *p* wave finds increasing difficulty in penetrating the centrifugal barrier associated with *p*-wave scattering. For example, the *p* wave contributes between 5% and 15% of the cross section at 50 meV impact energy, but less than 5% at 10 meV.

The *s*-wave scattering length $A_0$ is an important quantity used to characterize cold collisions. From a viewpoint riding on the unperturbed matter wave associated with the impacting electron far from the target, the wave appears to have its origin in the vicinity of the target, either in front of it ($A_0$ positive) or beyond it ($A_0$ negative). The distance between the apparent origin of the wave and the target is defined as the scattering length and is to some degree equivalent to the radius of the target that the molecule presents to the incoming electron. The absolute value of $A_0$ is given by $\mathbf{k}^{-1}\tan|\eta_0|$ as $\mathbf{k}\rightarrow0$. Figure 4 shows $\mathbf{k}^{-1}\tan|\eta_0|$ vs **k** between 9 and 70 meV, using *s*-wave phase shifts derived from the fitting procedure described above. The intercept on the vertical axis, obtained by simple extrapolation, yields a scattering length of $|6.28|\pm0.15$ in units of $a_0$ or $|3.32|\pm0.08$ Å. Equivalently, the scattering length may be determined from the limiting cross section as $\mathbf{k}\rightarrow0$, which is given by $4\pi A_0^2$. Extrapolation of our data gives a scattering length of $|6.22|a_0$ or $|3.29|$ Å.

A rapid rise in cross section at low energy and strong *s*-wave nature of the scattering in cold electron collisions are characteristic both of bound-state *s*-wave resonances, as in the formation of long-lived $SF_6^-$ [24] by $SF_6$, and in virtual-state scattering, with no accompanying long-lived negative ion formation. *S*-wave resonances have positive values of $A_0$ and virtual states have negative values. Our data may be used to distinguish between these two cases and to show that the scattering length in the present case is negative, as follows. We introduce the approximation that the long-range part of the interaction potential between the electron and $CO_2$ is dominated by spherically symmetrical charge-induced dipole polarization and thus by a potential varying as $r^{-4}$. Modified effective-range theory (MERT) then shows that [25,26]

$$\tan\eta_0=-A_0k\left[1+\left(\frac{4\alpha}{3a_0}\right)k^2\ln(ka_0)\right]-\left(\frac{\pi\alpha}{3a_0}\right)k^2+Dk^3+Fk^4, \tag{3}$$

$$\tan\eta_1=\left(\frac{\pi\alpha}{15a_0}\right)k^2+Hk^3, \tag{4}$$

where $\alpha$ is the polarizability of $CO_2$ ($=19.64a_0^3$) and $k$ and $A_0$ are expressed in units of $a_0^{-1}$ and $a_0$, respectively, where $a_0$ is the Bohr radius. Equations (3) and (4) yield *s*- and *p*-wave phase shifts which, inserted into Eqs. (1) and (2), yield integral and backward-scattering cross sections. Calculated cross sections were fitted to experimental values, using $A_0$, $D$, $F$, and $H$ as fitting parameters, noting that terms in $k^3$ and $k^4$ make only a small contribution. Using a negative value of $A_0$, good consistency could be obtained between integral and backward-scattering data. This is shown in Fig. 5 [fits labeled a and c], for data up to 50 meV with $A_0=-6.72a_0$, a value lying ~7% higher than the value recorded above (see Fig. 4). A positive value of the scattering length may also be used to fit the integral-scattering data, giving $A_0=6.04a_0$, but backward scattering is then strongly overestimated. This is also shown in Fig. 5 [fit labeled (b)]. It follows that $A_0$ is a negative quantity.

To reinforce this numerical analysis, it may be shown analytically using Eqs. (1)–(4) that the difference between the forward-scattering and backward-scattering cross sections $\Delta\sigma$ as a function of wave vector may be expressed as

$$\Delta\sigma\sim\frac{4\pi^2\alpha}{5}\left[-A_0k\left\{1+\frac{4\alpha}{3a_0}k^2\ln(ka_0)\right\}-\frac{\pi\alpha}{3a_0}k^2\right] \tag{5}$$

ignoring all terms involving fitted empirical coefficients of $k^3$ and $k^4$. Experimentally $\Delta\sigma$ is a positive quantity, with forward scattering dominating over backward, requiring that $A_0$ be negative. Hence we conclude that $A_0=-3.32\pm0.08$ Å, where the value from partial wave fitting is adopted since this, in contrast to MERT, requires no additional assumptions about the radial dependence of the interaction potential.

In addition, all calculations, both *ab initio* and based on model potentials, find a pole in the scattering matrix around zero real $k$, that is, around zero energy, but negative imagi-

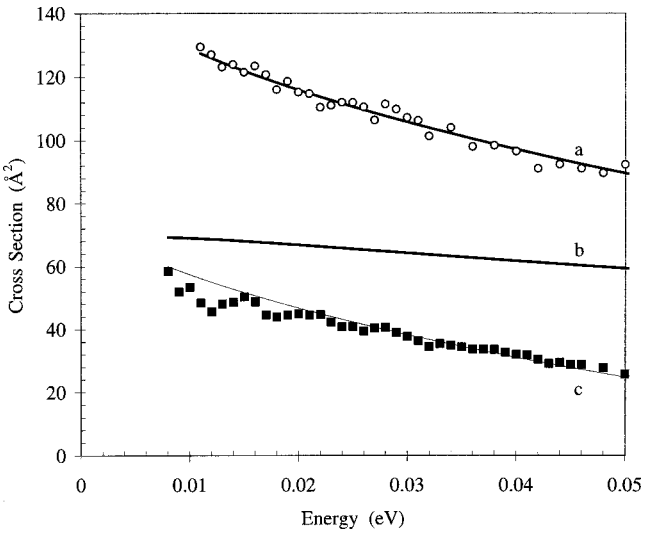


FIG. 5. Fits to experimental data, obtained using Eqs. (1)–(4), Sec. III. Fits are shown as continuous lines, experimental data for integral cross sections as open circles and backward scattering cross sections as filled squares. The fits labeled a and c were obtained with $A_0 = -6.72a_0$ and optimized coefficients $D$, $F$, and $H$ of $k^3$ and $k^4$ [Eqs. (3) and (4)]. The line labeled b represents the computed backward scattering cross sections obtained using a positive value of $A_0$, showing very poor agreement with experiment. Further details are given in Sec. III.

nary $k$ [3,4,23]. This represents the virtual state and requires that the scattering length be negative. By combining this robust qualitative theoretical result with our experimental data and with our derivation of negative scattering length above, the presence of the virtual state in electron-$CO_2$ scattering is very soundly established.

## IV. CONCLUDING REMARKS

Whilst it is unknown how widespread is the phenomenon of virtual-state scattering, the implications of our results go considerably beyond the issue of electron collisions with $CO_2$. For example, many of the same considerations, which govern cold electron collisions, also govern cold collisions of heavy particles. Thus cold molecular collisions could also show virtual-state elastic scattering. This may in fact have already been observed [27] in $Rb+Rb_2$ collisions, for which elastic scattering was found to have a large negative-scattering length in a Bose-Einstein condensate (BEC). In atom-atom collisions, strong enhancement of scattering in cold Cs-Cs collisions has been recorded at zero energy and this may also be attributable to a virtual state [28]. At all events, elastic collisions will play a central role in the formation of molecular BECs and the stability and properties of these condensates will depend on the sign and magnitude of the scattering length for elastic scattering [1]. Strong virtual-state cold molecule scattering would prohibit the formation of large condensates.

To conclude, returning to cold electron collisions, other nonpolar species such as benzene [15,29] and perhaps also naphthalene, anthracene, and perylene [30] may display virtual-state scattering near zero electron impact energy. Weakly dipolar species, with moments of less than $\sim$1 D, may also, in principle, show virtual-state scattering [31]. An example is $N_2O$, with a dipole moment of 0.161 D, which shows similar angular scattering behavior as $CO_2$ at 20 meV impact energy and anomalously high cross sections at low electron-collision energies (work in preparation). Vibrational and rotational excitation in cold collisions may also be enhanced by a virtual state, for example, for $CO_2$ [19,20,23], in which the departing inelastically scattered near-zero energy electron experiences the effect of the virtual state.

## ACKNOWLEDGMENTS

The authors would like to acknowledge valuable discussions with Knud Taulbjerg (Institute of Physics and Astronomy, University of Aarhus) on the interpretation of our data in terms of virtual-state scattering. We should also like to thank the Director and Staff at the Institute for Storage Rings at Aarhus (ISA) for providing the facilities necessary for this work.

[1] J. Weiner, V. S. Bagnato, S. Zilio, and P. Julienne, Rev. Mod. Phys. **71**, 1 (1999).
[2] L. A. Morgan, Phys. Rev. Lett. **80**, 1873 (1998).
[3] C.-H. Lee, C. Winstead, and V. McKoy, J. Chem. Phys. **111**, 5056 (1999).
[4] T. N. Rescigno, D. A. Byrum, W. A. Isaacs, and C. McCurdy, Phys. Rev. A **60**, 2186 (1999).
[5] J. L. Bohn, Phys. Rev. A **61**, 40702 (2000).
[6] M. A. Morrison, N. F. Lane, and L. A. Collins, Phys. Rev. B **15**, 2186 (1977).
[7] J. Ferch, C. Masche, and W. Raith, J. Phys. B **14**, L97 (1981).
[8] F. A. Gianturco and T. Stoecklin (private communication).
[9] S. Mazevet, M. A. Morrison, L. A. Morgan, and R. K. Nesbet (unpublished).
[10] R. K. Nesbet, S. Mazevet, and M. A. Morrison (unpublished).
[11] R. J. Gulley, S. L. Lunt, J.-P. Ziesel, and D. Field, J. Phys. B **31**, 2735 (1998).
[12] K. Radler and J. Berkowitz, J. Chem. Phys. **70**, 221 (1979).
[13] C. E. Kuyatt, in *Methods of Experimental Physics*, 7A, edited by B. Bederson and W. L. Fite (Academic, New York, 1968), Chap. 1, p. 43.
[14] G. Martinez, M. Sancho, and F. H. Read, J. Phys. E **6**, 631 (1983).
[15] J. Randell, S. L. Lunt, G. Mrotzek, J.-P. Ziesel, and D. Field, J. Phys. B **27**, 2369 (1994).
[16] R. E. Kennerly, Phys. Rev. A **21**, 1876 (1980).
[17] A. Hourri, J. M. St-Arnaud, and T. K. Bose, J. Chem. Phys. **106**, 1780 (1997).
[18] J. Randell, R. J. Gulley, S. L. Lunt, J. P. Ziesel, and D. Field, J. Phys. B **29**, 2049 (1996).

[19] K. H. Kochem, W. Sohn, N. Hebel, K. Jung, and H. Ehrhardt, J. Phys. B **18**, 4455 (1985).
[20] D. Field, S. L. Lunt, G. Mrotzek, J. Randell, and J.-P. Ziesel, J. Phys. B **24**, 3497 (1991).
[21] S. J. Buckman, M. T. Elford, and D. S. Newman, J. Phys. B **20**, 5175 (1987).
[22] H. Estrada and W. Domcke, J. Phys. B **18**, 4469 (1985).
[23] M. A. Morrison, Phys. Rev. A **25**, 1445 (1982).
[24] A. Chutjian and S. H. Alajajian, Phys. Rev. A **31**, 2885 (1985).
[25] T. F. O'Malley, Phys. Rev. **130**, 1020 (1963).
[26] S. J. Buckman, and J. Mitroy, J. Phys. B **22**, 1365 (1989).
[27] R. Wynar, R. S. Freeland, D. J. Han, C. Ryu, and D. J. Heinzen, Science **287**, 1016 (2000).
[28] M. Arndt, M. Ben Daham, D. Gury-Odelin, M. W. Reynolds, and J. Dalibard, Phys. Rev. Lett. **79**, 625 (1997).
[29] F. A. Gianturco and R. R. Lucchese, J. Chem. Phys. **108**, 6144 (1998), and private communication.
[30] D. Field, S. L. Lunt, S. V. Hofmann, and J.-P. Ziesel, in *Proceedings of the 3rd Cologne-Zermatt Symposium: The Physics and Chemistry of the Interstellar Medium. 1999*, edited by V. Ossenkopf (GCA Verlag, Herdecke, 1999).
[31] A. Herzenberg and B. C. Saha, J. Phys. B **16**, 591 (1983).